Journal of Power Sources 196 (2011) 2608–2614

Contents lists available at ScienceDirect

Journal of Power Sources

journal homepage: www.elsevier.com/locate/jpowsour

$Pt/Y_{0.16}Zr_{0.84}O_{1.92}/Pt$ thin film solid oxide fuel cells: Electrode microstructure and stability considerations

Kian Kerman*, Bo-Kuai Lai, Shriram Ramanathan

Harvard School of Engineering and Applied Sciences, Harvard University, Cambridge, MA 02138, USA

ARTICLE INFO

Article history:
Received 5 October 2010
Received in revised form 21 October 2010
Accepted 26 October 2010
Available online 3 November 2010

Keywords:
Micro-solid oxide fuel cell
Pt
Anode
Microstructure
Porosity
Thin films

ABSTRACT

Symmetric, free standing thin film micro-solid oxide fuel cells of $Pt/Y_{0.16}Zr_{0.84}O_{1.92}/Pt$ structure are studied in this report. The role of parameters such as electrolyte thickness and electrode porosity on fuel cell power output was investigated. A peak power density of 1037 mW cm^{-2} was exhibited with an optimized structure consisting of nano-porous Pt electrodes and 100 nm thick $Y_{0.16}Zr_{0.84}O_{1.92}$ with an open circuit voltage of 0.968 V at 500 °C using H_2 as fuel and standing air as the oxidant. A twelve hour test of these devices indicates that overall performance shows extreme sensitivity to microstructural changes in the pure metallic electrodes. Results presented herein enable mechanistic routes to performance optimization, provide device stability data and are relevant to advancing micro-fuel cells for portable energy.

1. Introduction

The demand for mobile energy is constantly growing in our society. Micro-fuel cells are considered promising portable power sources due to high energy densities [1]. This idea has motivated research on different types of micro-fuel cells, including micro-solid oxide fuel cells (μSOFCs) [2–13]. Though there has been decades of research on conventional solid oxide fuel cells (SOFCs), the novel and rigorous challenges of producing high performance thin film μSOFCs for low temperature applications are still in relatively early stages [11,14]. μSOFCs are comprised of thin film electrolytes and electrodes that can be integrated onto Si using semiconductor processing technology, making them an interesting field that has potential for facile manufacturing scale-up. Moreover, the large decrease in ohmic loss of thin electrolyte films in μSOFCs can greatly reduce the overall operating temperature, which is typically in the range of 800–1000 °C for conventional SOFCs. Benefits of decreased temperature operation to 500 °C range using thin film μSOFCs include reduced start-up time, mitigated material degradation or instability issues in stacking architectures, and potential practical realization of portable SOFCs [15].

Creating optimal porosity in metallic or ceramic–metal composite electrodes to mediate the electrochemical reactions occurring at triple phase boundaries (TPBs) is of essence for SOFC performance because both oxidation and reduction reactions occur only at TPBs between the oxidant or fuel, the electrode, and the electrolyte [16]. Further, it has recently been shown that porous anode microstructure plays a vital role in the overall performance of micro-tubular SOFCs [5]. Since the maximum power density in SOFCs is a convolution of many factors, a systematic evaluation of the main cell components, such as the electrodes and electrolyte, is essential to achieve optimal μSOFC performance. It is of particular importance to elucidate large variations, ranging several orders of magnitude, in performance of reported $Pt/(Y_2O_3)_{0.08}(ZrO_2)_{0.92}/Pt$ (Pt/YSZ/Pt) μSOFCs [2–4,7–13]. For example, Huang et al. [2] were able to achieve a maximal performance of 130 mW cm^{-2} at 350 °C in Pt/YSZ/Pt μSOFCs with 50 nm thick YSZ; while Rey-Mermet and Muralt [12,13] reported performance of 0.02 mW cm^{-2} at 500 °C using a 500 nm thick YSZ electrolyte. Fig. 1 graphically depicts performance of planar Pt/YSZ/Pt thin film μSOFCs that various research groups have reported thus far. Though device fabrication methods and thin film deposition techniques vary amongst researchers, a systematic evaluation of performance governing factors in Pt/YSZ/Pt μSOFCs has not yet been addressed in detail. Furthermore, there is no discussion on the stability or operational status of these devices.

Similar to conventional SOFCs, μSOFCs can potentially operate on hydrogen (H_2) or hydrocarbons, depending on the anode material used. The ability to directly use methane (CH_4) is greatly desired, as it is a much more abundant and economically viable fuel compared to H_2. Efforts have been made in addressing the design of potential anode materials for direct hydrocarbon utilization in

* Corresponding author. Tel.: +1 617 497 2746.
E-mail address: kkerman@fas.harvard.edu (K. Kerman).

0378-7753/$ – see front matter © 2010 Elsevier B.V. All rights reserved.
doi:10.1016/j.jpowsour.2010.10.068

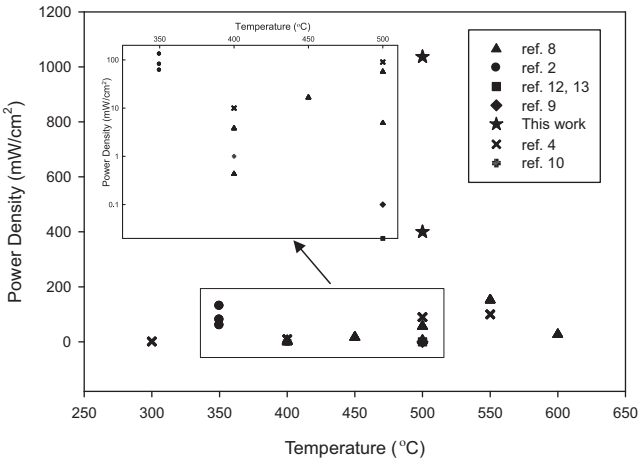

Fig. 1. Representation of the variation in overall planar thin film Pt/YSZ/Pt μSOFC performance reported in the literature to date [2,4,8–10,12,13]. The inset shows a zoomed in semi-log plot of the region highlighted.

SOFCs [17–19]; however there has been no demonstration of low temperature, direct CH_4 utilization in thin film-based oxide fuel cells.

In this study, we report the direct effects of sputtered electrode porosity and electrolyte thickness on μSOFC performance. We present a deterministic route towards μSOFC performance enhancement that is relevant to fuel cells utilizing porous electrodes and may elucidate the extreme variation in performance reported in the literature. Using this approach, we were able to achieve a maximum power density of 1037 mW cm^{-2} at 500 °C with H_2 and demonstrate functionality in CH_4 at reduced temperatures. Moreover, we investigate the fixed temperature stability of such devices and discuss mechanisms leading to performance changes.

2. Experimental

YSZ electrolyte films were grown by radio-frequency sputtering at a power of 100 W from a stoichiometric target in 5 mTorr Ar at a substrate temperature of 550 °C. The corresponding deposition rate was 1.2 nm min^{-1}. Films deposited under these conditions led to the proper compressive stress regime [20–22] necessary for free standing membrane stability. Porous Pt films were grown from an elemental Pt target by sputtering in 75 mTorr Ar without substrate heating.

Plan view transmission electron microscope (TEM) samples were prepared by manual polishing of the underlying substrate, then ion milling to electron transparency using a Fischione 10-10 dual-beam ion mill. A JEOL 2100 was used to investigate the local grain structure and crystallinity of YSZ electrolyte films. A Zeiss Supra 55VP scanning electron microscope (SEM) was used to characterize the porous electrode structure of the μSOFCs. Quantitative porosity investigations were possible due to the single layer, nano-structured thin films grown. Porosity estimates were made by converting SEM micrographs to binary images, thresholding, and gathering pixel ratios with the National Institutes for Health software, ImageJ.

μSOFC devices were produced in the following manner: patterning of double side Si_3N_4 coated Si wafers with photolithography, removal of patterned Si_3N_4 by reactive ion etching, selective

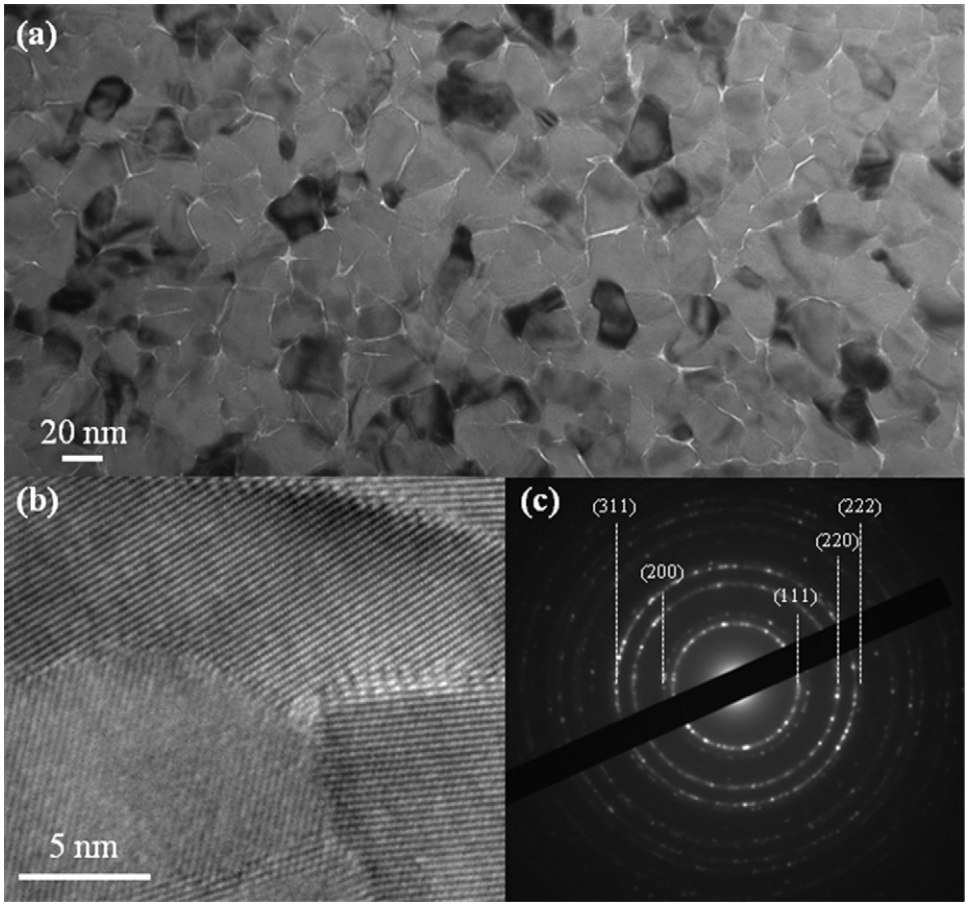

Fig. 2. (a) Bright field TEM and (b) high resolution TEM showing nanostructured YSZ films, while (c) indexed (ICDD 030-1468) selected area electron diffraction confirms a cubic single phase has been formed.

area etching of exposed Si with a 30 wt.% KOH aqueous solution, deposition of YSZ electrolyte and Pt cathode on the free standing planar Si_3N_4 membrane surface, removal of Si_3N_4 from the below by reactive ion etching, and finally deposition of the Pt anode on Si well side. More extensive technical detail on this fabrication method can be found in previous works [2,4,20,22]. μSOFC performance was tested in a custom measurement station with argon carrier gas containing 5% wet hydrogen or 5% wet methane as fuel and stationary air as the oxidant [4].

3. Results and discussion

A plan view bright field TEM image in Fig. 2a shows the nanogranular structure of the YSZ electrolyte thin films. The average grain size was estimated to be approximately 15 nm. The high resolution TEM image (Fig. 2b) indicates that there are no visible amorphous intergranular impurities in the films, while the selected area electron diffraction pattern (Fig. 2c) confirms that the YSZ films are single phase and cubic. The electrocatalyst used as both the anode and cathode in this study was Pt. It should be noted that although Pt may be a cost prohibitive catalyst for widespread use, a total Pt loading on each electrode of less than 1.7 μg cm^{-2} was used for the μSOFCs studied. As a rough comparison, conventional proton exchange membranes typically use Pt loadings in the hundreds of μg cm^{-2} range [23,24]. In addition, by using Pt, de-convolution of possible reaction mechanism pathways is greatly simplified. Since the purely metallic catalyst electrode does not allow ionic conduction, there can be only one dominant path for O_2 reduction at the cathode and H_2 oxidation at the anode, namely at the TPBs.

To study the effect of electrolyte thickness, a series of three μSOFCs with YSZ thicknesses of 27, 54, and 108 nm were fabricated with similar Pt electrodes. The open circuit voltage (OCV) under measurement conditions of these μSOFCs is shown in Fig. 3, while Fig. 3a illustrates an optical micrograph of the fabricated μSOFC membrane showing a characteristic compressive buckling pattern. The closeness of the OCVs to the thermodynamic limit, or the Nernst potential, in the temperature range tested confirms the high quality nature of the free standing YSZ electrolyte films, which is essential for high-performance fuel cells. We do note here that one can see variation in the OCV, including deviations from the Nernst potential of up to 200 mV. Reasons for this deviation may be related to slight fuel leakage between the anode and cathode. However, even in the case of the 27 nm thick YSZ μSOFC, an excellent chemical potential is maintained throughout the temperature range investigated.

To evaluate the significance of overall porosity to μSOFC performance, several different Pt electrodes were synthesized. Fig. 4a illustrates the relationship of Pt film thickness to porosity for films grown under similar conditions in both the cathode and anode. Since the average pore size for all samples was approximately equal to within one standard deviation, the total porosity is an indication of overall TPB length. It can be seen that the different electrodes exhibit markedly dissimilar trends in porosity. This is a direct result of the micro-fabrication method used to synthesize μSOFCs, as it is well known that the deposition surface and atmosphere play a key role in the structure of thin metallic films on oxides [25]. As described in Section 2, the cathode deposition is on a planar surface, whereas the anode deposition occurs within a

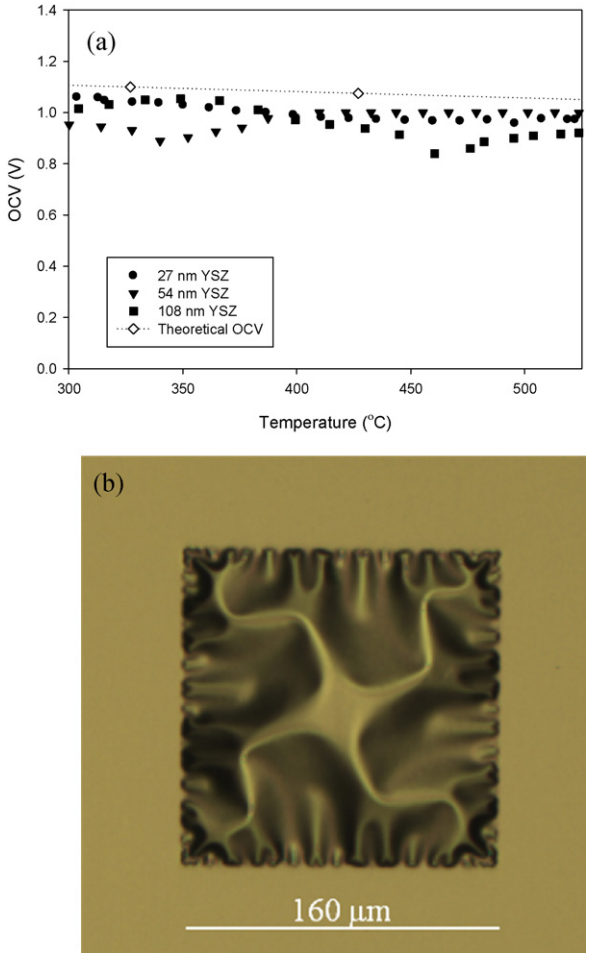

Fig. 3. (a) Measured OCV with 80 nm Pt electrodes in Pt/YSZ/Pt μSOFCs with varying thickness electrolytes as a function of temperature and (b) optical image of μSOFC.

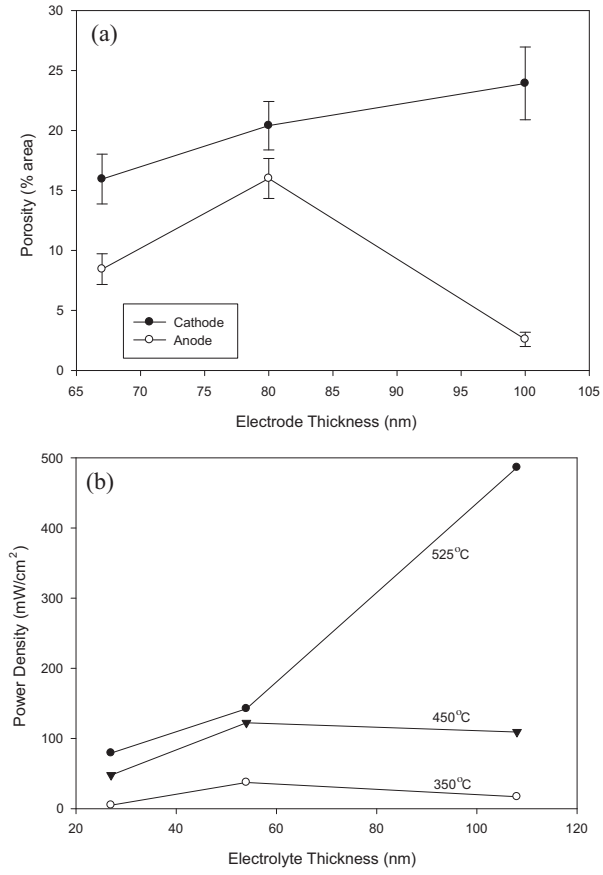

Fig. 4. (a) Effect of Pt thickness on porosity for the cathode and anode in Pt/YSZ/Pt μSOFCs and (b) effect of electrolyte thickness on 80 nm Pt electrodes in Pt/YSZ/Pt μSOFCs at 350 °C, 450 °C, and 525 °C.

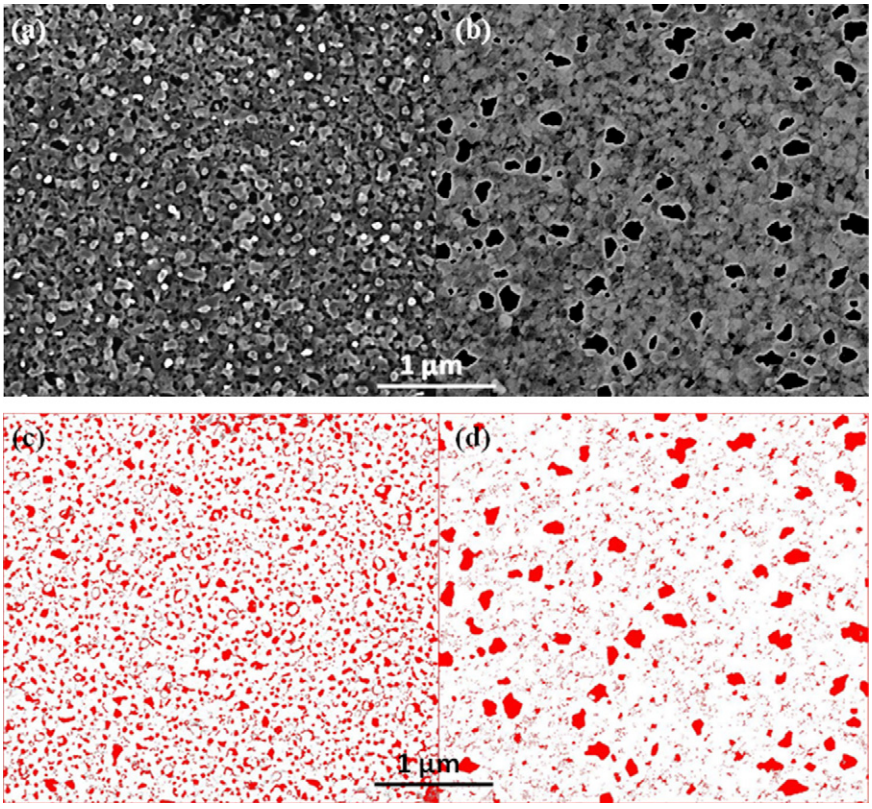

Fig. 5. Post fuel cell measurement SEM micrographs and corresponding binary converted image of anode with (a), (c) increased TPB perimeter with 19% area porosity and (b), (d) anode with 16% area porosity.

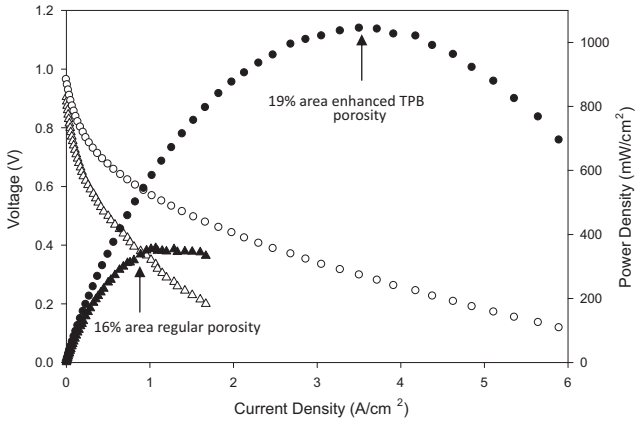

Fig. 6. Performance of two 80 nm Pt/YSZ/Pt at 500 °C using 5% wet H_2 as fuel, with open and closed symbols for voltage and power density, respectively.

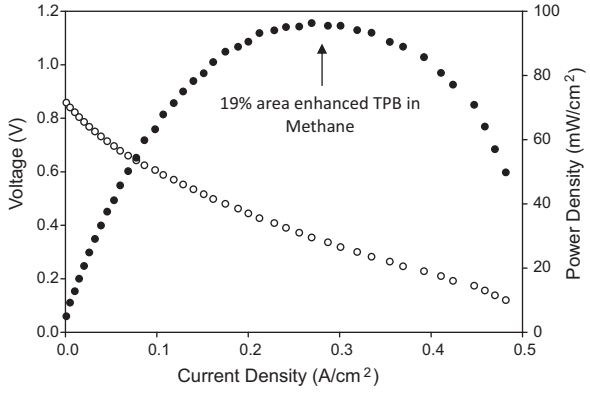

Fig. 7. Performance of 80 nm Pt/YSZ/Pt with optimal structure at 440 °C operating with 5% wet CH_4 as fuel. Open and closed symbols are for voltage and power density, respectively.

confined Si well after patterning. Therefore, it is not unreasonable to expect different adatom arrangement processes for the anode and cathode. 80 nm thick Pt electrodes with approximately 16% porosity were used to further investigate the effect of electrolyte thickness on μSOFC performance. Fig. 4b shows the relationship of electrolyte thickness and maximum power density at several temperatures. It can be seen that there is not a simple monotonic relationship with increasing temperature. In the low temperature regime, it appears that YSZ at the intermediate thickness of ~50 nm gives maximal performance, similar to the reports in Ref. [2]. However, there is a clear shift that occurs at higher temperatures, in which thicker YSZ of ~100 nm performs much better. This result is counterintuitive, as one may expect a proportional relationship between scaling of electrolyte thickness and performance [2,7,14]. A possible reason for the observed behavior is that one of the competing performance-limiting factors such as fuel permeation or area

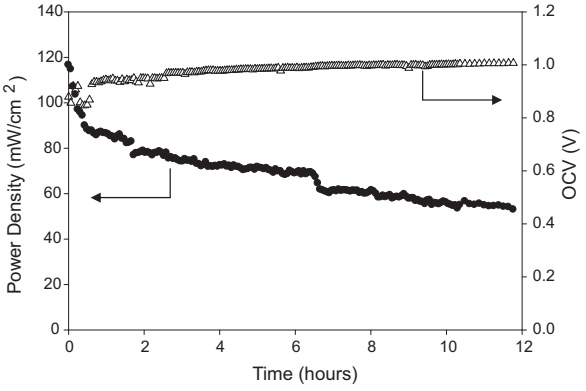

Fig. 8. Overall performance and OCV of a Pt/YSZ/Pt μSOFC at 400 °C operating continuously for 12 h with 5% wet H_2 as fuel. Open and closed symbols are for voltage and power density, respectively.

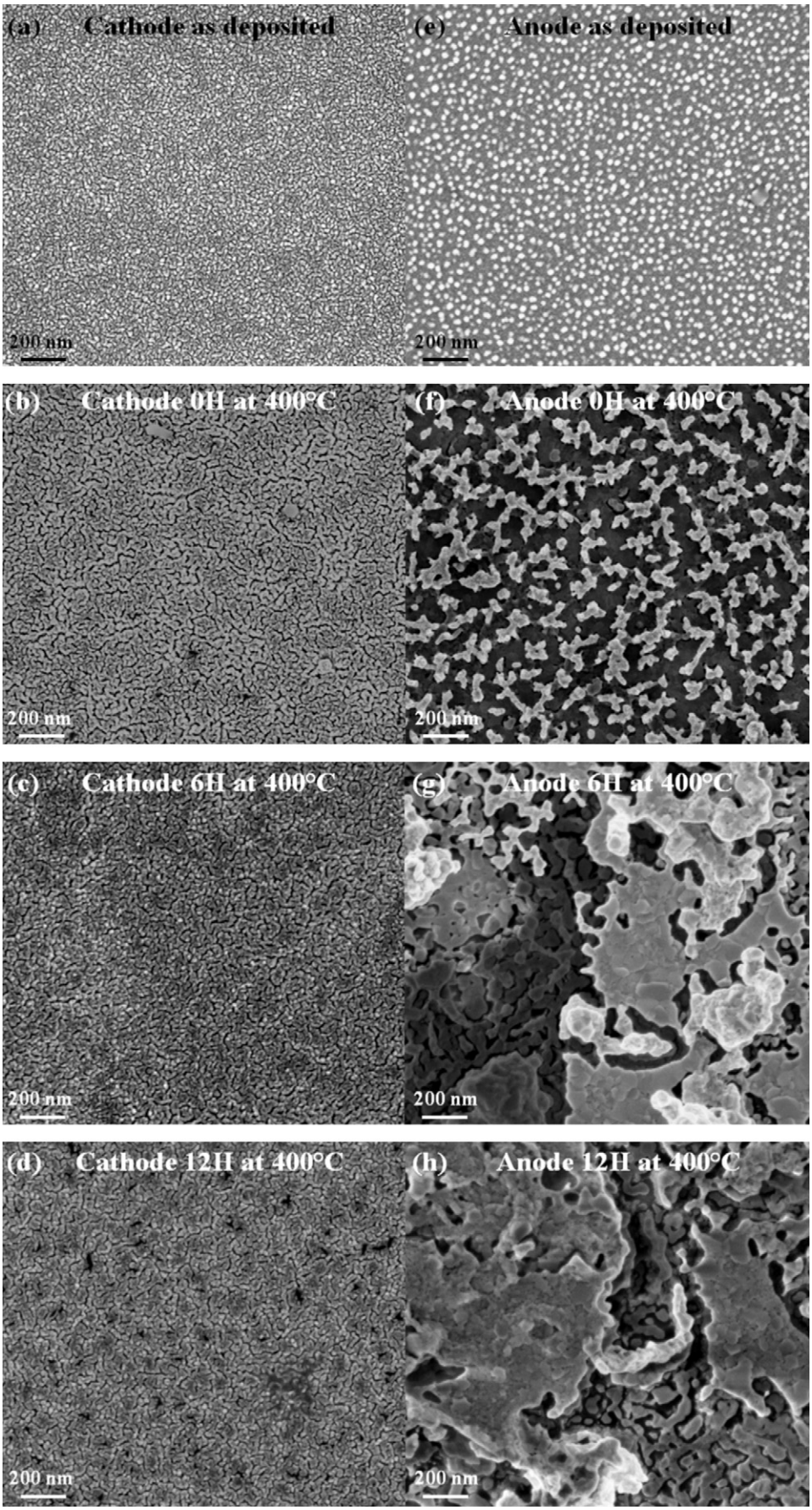

Fig. 9. (From top to bottom) SEM micrographs of the cathode (a)–(d) and anode (e)–(h) as-deposited, heated up to 400 °C, 6 h at 400 °C, and 12 h at 400 °C.

specific resistance begins to dominate in a particular temperature regime.

To demonstrate the significance of TPB length in porous electrode structures for μSOFCs, using the 108 nm thick YSZ electrolyte, two alternate anodes were grown. Fig. 5a–d shows the SEM micrographs and accompanying binary converted images (thresholded) of two different 80 nm Pt anodes after measurement having similar total porosity, but distinctly different average pore size. Clearly the total perimeter of porous regions, i.e. TPB length, in the Pt film with smaller average pore size is larger than that of its counterpart. Since the anodic reaction, $H_2 + O^{2-} \rightarrow H_2O + 2e^-$, occurs at the TPBs and Pt electrodes are well interconnected, it follows that exchange current density and TPB length will be directly proportional. Thus by increasing the TPB length in the μSOFC anode, one can expect a direct performance enhancement. Additionally, we have experimentally isolated the role of the TPB in the anode by leaving the Pt cathode structure unchanged for the two μSOFCs under comparison. In Fig. 6 we report the maximum power density obtained at 500 °C for two cells with similar total porosity in the anode and cathode, but different TPB lengths on the anodes. Over a two-fold increase in power density is observed by reducing the average pore size by approximately two times and therefore increasing the TPB length. A power density of 1037 mW cm^{-2} was obtained at 500 °C in this near-ideal μSOFC structure with an OCV of 0.968 V. To the best of the authors' knowledge this is the highest performance reported to date for thin film Pt/YSZ/Pt planar μSOFCs, most of which are outlined in Fig. 1. As a proof-of-concept to illustrate fuel versatility in μSOFCs, Fig. 7 shows the optimal μSOFC structure tested with CH_4 as fuel. It is known that the addition of Pt in typical Ni-YSZ composite anodes aids in the reforming of CH_4 and reduces the potential for coking [26]; though pure Pt is not an ideal catalyst for direct oxidation of CH_4. A maximum power density of 95 mW cm^{-2} at 440 °C was obtained. This result is an order of magnitude lower than that with H_2 fuel. As detailed below, the microstructure of the Pt anodes was found to be unstable in a reducing atmosphere, which may have contributed to the performance decrease. This is however, the first demonstration of a micro-SOFC operating at low temperatures with CH_4 used directly as a fuel and an encouraging result for advancing new materials research towards designing stable anodes for direct hydrocarbon utilization at reduced temperatures.

The stability of these μSOFCs was tested by keeping the cell under measurement conditions for 12 h. Fig. 8 shows the evolution of the μSOFC OCV and power density as a function of time, while being held at a constant temperature of 400 °C. It can be seen that the potential across the μSOFC is relatively stable, indicating that there is little change in the dense electrolyte separating the anode and cathode. The power density variation indicates that there are substantial microstructural changes occurring in the device components. Performance degradation seen in these μSOFCs indicates instability in electrode microstructures. After 12 h of testing, the power density of the cell dropped to about 50% of its initial value. SEM micrographs of the anode and cathode are shown as-deposited, after initial heating to temperature, and at 6 h intervals in Fig. 9a–h. It should be noted that the cell used for microstructural investigation by SEM was not the same cell used for performance measurement, therefore, only the effect of elevated temperature in a reducing or oxidizing environment can be attributed for the microstructural change observed in Fig. 9. However, it is known that high current density in Pt, specifically at TPB interfaces, can play additional role in morphology changes [27,28]. Clearly, there is a difference between elevated temperature exposure on the anode and cathode. In fact, in air, the cathode seems largely unaffected by the high temperature anneal. Conversely, the anode goes through very interesting microstructural changes, likely due to the coupled effect of elevated temperature and a reducing environment. As seen in the SEM micrographs of the anode (Fig. 9e–h), Pt coarsening induced by surface energy minimization results in a large decrease in overall porosity. This leads to the catalytic properties for oxidation associated with Pt/YSZ boundaries being reduced and is manifested by a lowering of measured power density. Indeed, it has been shown that Pt can be unstable at elevated temperatures, but small amounts of Ni doping may enhance its high temperature stability [10]. Similar to stable conventional SOFCs that can operate for hundreds of hours without degradation, ceramic materials able to act as mixed conductors [22] at reduced temperatures may warrant further investigation to address the long term feasibility of thin film μSOFCs.

4. Conclusion

We have shown that superior performance in low temperature planar μSOFCs is attainable by careful tuning of porous electrode microstructures and electrolyte thickness. It was found that overall performance shows extreme sensitivity to Pt anode porosity and microstructure. The overall Pt loading for each electrode in the μSOFCs studied here was approximately 1.7 μg cm^{-2}, which is in or below the typical range for proton exchange membranes. The following is a brief summary of the results presented in this study:

1. A systematic approach to achieving high performing μSOFCs led to an optimization of electrolyte thickness, electrode total porosity, and insights into the effect of porosity size distribution. These results should elucidate the variations in performance of Pt/$(Y_2O_3)_{0.08}(ZrO_2)_{0.92}$/Pt μSOFCs presented in the literature thus far.
2. A maximum power density of 1037 mW cm^{-2} at 500 °C was obtained in Pt/$(Y_2O_3)_{0.08}(ZrO_2)_{0.92}$/Pt μSOFCs with an 80 nm thick electrode exhibiting 19% total porosity and a 108 nm electrolyte using 5% wet H_2 as fuel and stationary air as the oxidant.
3. Demonstration of low temperature μSOFC functionality with methane as fuel was shown at temperatures below 500 °C. A maximum power density of 95 mW cm^{-2} at 440 °C was achieved using 5% CH_4.
4. Overall stability of Pt/$(Y_2O_3)_{0.08}(ZrO_2)_{0.92}$/Pt μSOFC structures was investigated. 12 h of continuous use indicated that purely metallic electrodes such as Pt exhibit great sensitivity to a high temperature reducing atmosphere. Power density was found to reduce by approximately 50% at 400 °C after 12 continuous hours of testing.

We anticipate these results could be of relevance to advancing the development of stable, high performance thin film solid oxide fuel cells operating at reduced temperatures.

Acknowledgment

The authors acknowledge National Science Foundation for financial support.

References

[1] C.K. Dyer, J. Power Sources 106 (2002) 31–34.
[2] H. Huang, M. Nakamura, P.C. Su, R. Fasching, Y. Saito, F.B. Prinz, J. Electrochem. Soc. 154 (2007) B20–B24.
[3] A. Bieberle-Hütter, D. Beckel, A. Infortuna, U.P. Muecke, J.L.M. Rupp, L.J. Gauckler, S. Rey-Mermet, P. Muralt, N.R. Bieri, N. Hotz, M.J. Stutz, D. Poulikakos, P. Heeb, P. Muller, A. Bernard, R. Gmur, T. Hocker, J. Power Sources 177 (2009) 123–130.
[4] A.C. Johnson, B.-K. Lai, H. Xiong, S. Ramanathan, J. Power Sources 186 (2009) 252–260.
[5] T. Suzuki, Z. Hasan, Y. Funahashi, T. Yamaguchi, Y. Fujishiro, M. Awano, Science 325 (2009) 852–855.
[6] Z. Shao, S.M. Haile, Nature 431 (2004) 170–173.
[7] A. Ignatiev, X. Chen, N.J. Wu, Z.G. Lu, L. Smith, Dalton Trans. 40 (2008) 5501–5506.

[8] U.P. Muecke, D. Beckel, A. Bernard, A. Bieberle-Hütter, S. Graf, A. Infortuna, P. Müller, J.L.M. Rupp, J. Schneider, L.J. Gauckler, Adv. Funct. Mater. 18 (2008) 3158–3168.
[9] N. Yamamoto, D.J. Quinn, N. Wicks, J.L. Hertz, J. Cui, H.L. Tuller, B.L. Wardle, J. Micromech. Microeng. 20 (2010) 035027.
[10] X. Wang, H. Huang, T. Holme, X. Tian, F.B. Prinz, J. Power Sources 175 (2008) 75–81.
[11] A. Evans, A. Bieberle-Hütter, J.L.M. Rupp, L.J. Gauckler, J. Power Sources 194 (2009) 119–129.
[12] S. Rey-Mermet, P. Muralt, Solid State Ionics 179 (2008) 1497–1500.
[13] S. Rey-Mermet, Microfabricated solid oxide fuel cells, PhD Thesis, 2008.
[14] S.J. Litzelman, J.L. Hertz, W. Jung, H.L. Tuller, Fuel Cells 8 (2004) 294–302.
[15] A. Weber, E.I. Tiffee, J. Power Sources 127 (2004) 273–283.
[16] S.C. Singhal, K. Kendall, High Temperature Solid Oxide Fuel Cells, Elsevier, Oxford, UK, 2003.
[17] A. Atkinson, S. Barnett, R.J. Gorte, J.T.S. Irvine, A.J. McEvoy, M. Mogensen, S.C. Singhal, J. Vohs, Nat. Mater. 3 (2004) 17–27.
[18] Y.-H. Huang, R.I. Dass, Z.-L. Xing, J.B. Goodenough, Science 312 (2006) 254–257.
[19] S. Tao, J.T.S. Irvine, Nat. Mater. 2 (2003) 320–323.
[20] C.D. Baertsch, K.F. Jensen, J.L. Hertz, H.L. Tuller, S.T. Vengallatore, S.M. Spearing, M.A. Schmidt, J. Mater. Res. 19 (2004) 2604–2615.
[21] B.-K. Lai, K. Kerman, S. Ramanathan, J. Power Sources 195 (2010) 5185–5196.
[22] B.-K. Lai, K. Kerman, S. Ramanathan, J. Power Sources (2010), doi:10.1016/j.jpowsour.2010.09.066.
[23] M. Lefèvre, E. Proietti, F. Jaouen, J.-P. Dodelet, Science 324 (2009) 71–74.
[24] H.A. Gasteiger, J.E. Panels, S.G. Yan, J. Power Sources 127 (2004) 162–171.
[25] C.T. Campbell, Surf. Sci. Rep. 27 (1997) 1–111.
[26] T. Takeguchi, R. Kikuchi, T. Yano, K. Eguchi, K. Murata, Catal. Today 84 (2003) 217–222.
[27] J. Nielsen, T. Jacobsen, Solid State Ionics 178 (2007) 1001–1009.
[28] E. Mutoro, S. Günther, B. Luerßen, I. Valov, J. Janek, Solid State Ionics 179 (2008) 1835–1848.